Biogeosciences Discuss., https://doi.org/10.5194/bg-2017-256
Manuscript under review for journal Biogeosciences
Discussion started: 27 June 2017

Biogeosciences
Discussions
Open Access

Glacial-Interglacial changes and Holocene variations in Arabian Sea denitrification

Birgit Gaye[1], Anna Böll[1], Joachim Segschneider[2], Nicole Burdanowitz[1], Kay-Christian Emeis[1,3], Venkitasubramani Ramaswamy[4], Niko, Lahajnar[1], Andreas Lückge[5] and Tim Rixen[1,6]

[1]Institute for Geology, Universität Hamburg, Bundesstraße 55, 20146 Hamburg, Germany
[2]Institute for Geosciences, Universität Kiel, Ludewig-Meyn-Straße 10, 24118 Kiel, Germany
[3]Institute of Coastal Research, Helmholtz Center Geesthacht, Max-Planck-Straße 1, 21502 Geesthacht, Germany
[4]National Institute of Oceanography, Dona Paula, Goa, 403004, India
[5]Bundesanstalt für Geowissenschaften und Rohstoffe, Stilleweg 2, 30655 Hannover, Germany
[6]Leibniz-Zentrum für Marine Tropenforschung (ZMT) GmbH, Fahrenheitstraße 6, 28359 Bremen, Germany

Abstract

At present the Arabian Sea has a permanent oxygen minimum zone (OMZ) at water depths between about 100 m and 1200 m. Active denitrification in this OMZ is recorded by enhanced $\delta^{15}N$ values in the sediments. Sediment cores show a $\delta^{15}N$ increase from early to late Holocene which is contrary to the trend in other regions of water column denitrification. We calculated composite sea surface temperature (SST) and $\delta^{15}N$ in time slices of 1000 years of the last 25 ka to better understand the reasons for the establishment of the Arabian Sea OMZ and its response to changes in the Asian monsoon system. Pleistocene stadial $\delta^{15}N$ values of 4-6 ‰ suggest that denitrification was inactive or weak. During interstadials (IS) and the entire Holocene, $\delta^{15}N$ values of > 7 ‰ indicate enhanced denitrification and a stronger OMZ. This coincides with active monsoonal upwelling along the western margins of the basin as indicated by low SST. Stronger ventilation of the OMZ in the early to mid-Holocene period during the most intense southwest monsoon and vigorous upwelling is reflected in lower $\delta^{15}N$ compared to the late Holocene. The displacement of the core of the OMZ from the region of maximum productivity in the western Arabian Sea to its present position in the northeast was established during the last 4-5 ka. This was probably caused by (i) rising oxygen consumption due to enhanced northeast monsoon driven biological productivity, in combination with (ii) reduced ventilation due to a longer residence time of OMZ waters.

1 Introduction

The marine nitrogen (N) cycle is highly dynamic due to the many chemical compounds of reactive N and their rapid transformation processes. Its feed-back mechanisms are able to respond to external perturbations, possibly stabilizing the marine inventory of fixed N (Deutsch et al., 2004; Gruber, 2008; Sigman et al., 2009). The range of both oceanic N sources and sinks are still uncertain due to the poor data coverage of rate measurements and the large uncertainties of the water mass ages. The estimates of total N sources and sinks vary by factors of up to four and it has been debated whether the recent marine N cycle is in balance (Brandes and Devol, 2002; Codispoti, 2007; Codispoti et al., 2001; Gruber, 2008; Gruber and Sarmiento, 1997). Models have constrained the major oceanic N sinks (total water column and benthic denitrification) to 120-240 Tg N a^{-1} and brought them close to equilibrium with estimates of diazotrophic N fixation, the main oceanic N source (Deutsch et al., 2004; DeVries et al., 2013). New measurements have at the same time led to higher global estimates of N_2-fixation (Grosskopf et al., 2012).

A period of fundamental change of oceanic N cycling (among other element cycles) occurred during the transition from the last deglaciation to the early to mid-Holocene due to adjustment to changes in ocean circulation and nutrient as well as trace metal supply from land (Deutsch et al., 2004; Eugster et al., 2013). The present equilibrium was probably attained only a few thousand years ago (Deutsch et al., 2004; Eugster et al., 2013). Understanding the response of the N cycle to this complex reorganization is important to facilitate our present understanding of N cycling on global as well as regional scales (Gruber and Galloway, 2008).

Sedimentary $\delta^{15}N$ values allow a reconstruction of changes in N cycling. Denitrification strongly fractionates N isotopes, and the residual nitrate has $\delta^{15}N$ above the oceanic average of 5 ‰ (Brandes et al., 1998; Cline and Kaplan, 1975). Convective mixing and especially upwelling force nitrate-deficient water masses to the surface, so that the high $\delta^{15}N$ signal of nitrate is effectively transported into the euphotic zone. After assimilation into biomass by phytoplankton, ^{15}N-enriched particulate matter sinks through the water column to the seafloor where the signal of denitrification and OMZ intensity is preserved in the sediments (Altabet et al., 1995; Gaye-Haake et al., 2005; Naqvi et al., 1998; Suthhof et al., 2001). The nitrogen deficit produced by denitrification can be counteracted by dinitrogen (N_2) fixation from the atmosphere, which introduces nitrogen with a δ^{15}N only slightly lower than the atmospheric value of 0 ‰, as the process is associated with little isotopic fractionation (Carpenter et al., 1997).

Sedimentary δ^{15}N records show that during the last glacial maximum (LGM; 26-19 ka BP) denitrification was less intense than today (Galbraith et al., 2013). Models suggest - albeit with many uncertainties and unknowns - that both denitrification and N_2 fixation were lower during the LGM (Deutsch et al., 2004; Eugster et al., 2013; Galbraith et al., 2013; Schmittner and Somes, 2016). However, due to a stronger reduction of denitrification than of N_2 fixation, total export production was higher and increased the glacial oceanic N inventory by 10-50 % over that of the Holocene, affecting also the carbon storage in the ocean (Deutsch et al., 2004; Eugster et al., 2013; Schmittner et al., 2007).

Distinct changes of sedimentary δ^{15}N values (Galbraith et al., 2013) during deglaciation are interpreted to reflect the major changes in the N inventory. The decreasing iron supply at the end of the LGM may have significantly reduced N_2 fixation, leading to a rise of δ^{15}N even during the LGM (Eugster et al., 2013). Enhanced upwelling at about 15 ka BP led to abrupt onsets or increases of denitrification in the eastern tropical north and south Pacific as well as in the Arabian Sea (Altabet et al., 1995; Deutsch et al., 2004; Ganeshram et al., 2000; Ganeshram et al., 1995; Suthhof et al., 2001). The corresponding signal of enhanced δ^{15}N values was registered in many parts of the global ocean from the late glacial to early Holocene and was followed by a smooth decrease of δ^{15}N induced by the delayed increase of benthic denitrification caused by sea level rise (Deutsch et al., 2004; Galbraith et al., 2013; Ren et al., 2012). This sequence of events is very well recorded in cores from the east Pacific upwelling areas, but differs from the temporal pattern seen in sedimentary records from the Arabian Sea that show stable or increasing δ^{15}N values in the late Holocene (Galbraith et al., 2013).

In order to (i) discern why N cycling in the Arabian Sea differs from the global trend and to (ii) better understand the response of the OMZ to changes in the monsoon system we present a summary of δ^{15}N-records from the Arabian Sea including two new records from the Oman upwelling area (Table 1; Fig. 1a). The records are from different areas and trace the regional history of mid-water oxygenation over the last 25 ka. To relate the records of mid water oxygenation to the history of southwest (SW) monsoon upwelling and northeast (NE) monsoon winter cooling, we compiled SST records from the literature and generated a new temperature reconstruction for the Oman upwelling area (Table 1; Fig. 1b). Based on these integrated SST- and δ^{15}N-records for different regions of the Arabian Sea we examine contrasts between Last Glacial and Holocene conditions over the entire basin, and contrasting regional evolution within the basin during the Holocene. Finally, we discuss our conclusions with results of the global climate and ocean biogeochemistry model (KCM/PISCES) for the Holocene Arabian Sea.

2 Material and Methods

2.1 Study Area

The Arabian Sea hosts one of the most pronounced mid-water OMZ of the world's ocean and is a major oceanic N sink due to denitrification, anammox or dissimilatory nitrate reduction to ammonium (DNRA) in the OMZ (Bulow et al., 2010; Codispoti et al., 2001; Gaye et al., 2013a; Jensen et al., 2011; Ward et al., 2009). Suboxic conditions between the thermocline and 1200 m are maintained by the balanced interaction of oxygen demand (organic matter

Biogeosciences Discuss., https://doi.org/10.5194/bg-2017-256
Manuscript under review for journal Biogeosciences
Discussion started: 27 June 2017

degradation) and oxygen supply (ventilation; e.g., Olson et al., 1993; Sarma, 2002). The degradation of organic matter sinking out of the surface mixed layer consumes oxygen in the upper sub-thermocline water column. Primary productivity and particle flux in the Arabian Sea are highly seasonal and more than 50 % of annual particle fluxes occur during the summer season (Haake et al., 1993; Nair et al., 1989; Rixen et al., 1996), when strong SW monsoon winds induce upwelling of cold, nutrient-rich water masses along the coast of Somalia and Oman (Fig. 2a). The northeastern Arabian Sea off Pakistan has its temperature minimum and productivity maximum during the NE monsoon (January to March; Fig. 2b) caused by deep convection due to winter cooling (Rixen et al., 2005; Wiggert et al., 2000).

The main sources of oxygen for intermediate waters in the northern Arabian Sea are the outflows from the marginal seas (Red Sea, Persian Gulf) in the north and Indian Ocean Central Water (IOCW) from the south (Olson et al., 1993). Persian Gulf Water (PGW; 200-400 m water depth) and Red Sea Water (RSW; 600-800 m water depth) have high salinities and are saturated with oxygen from atmospheric contact shortly before their passage into the Arabian Sea through the Strait of Hormuz (50 m sill depth) and Strait of Bab-el-Mandeb (137 m sill depth), respectively (Rohling and Zachariasse, 1996; Sarma, 2002). IOCW combines Antarctic Intermediate Water, Subantarctic Mode Water and Indonesian Intermediate Water and is transported to the northern Arabian Sea from the southwest as part of the Somali current (Resplandy et al., 2012, You, 1998). Intermediate water from the southern sources is originally rich in oxygen, but becomes increasingly oxygen depleted and nutrient rich on its path to the Arabian Sea owing to oxygen loss during the mineralization of sinking organic matter. Progressive oxygen loss is reflected by the observed pattern with higher oxygen concentrations in the NW basin than in the NE basin of the Arabian Sea.

The intensity of the OMZ and denitrification is seasonally variable. Oxygen concentrations in its core and its volume vary in response to the seasonality of ventilation probably related to the seasonality of isopycnal mixing (Banse et al., 2014; Rixen et al., 2014). Models produce similar patterns with major ventilation from the south during the SW monsoon while reversing currents, consumption and isopycnal mixing reduce oxygen concentrations in the entire basin during the winter monsoon (Resplandy et al., 2012; Rixen et al., 2014). Reoxygenation during the SW monsoon occurs via the invigorated Somali current in the western Arabian Sea and a northward flowing undercurrent below 150 m water depth along the SW coast of India (Resplandy et al., 2012). Vertical as well as horizontal eddy advection, are additional important drivers of OMZ ventilation (Resplandy et al., 2012). At present, strongest denitrification prevails in the NE Arabian Sea although productivity and particle fluxes are highest in the western part of the basin (Gaye-Haake et al., 2005, Naqvi et al., 1990). Denitrification, that reduces nitrate to nitrite and gaseous dinitrogen, is triggered when oxygen concentrations fall below 5µM O_2 (Devol, 1978). In general, oxygen deficient conditions enable denitrification below 100 m water depth in the Arabian Sea (Gaye et al., 2013a). The intrusion of PGW that flows in a southward direction along the coast of Oman can occasionally supply oxygen and suppress denitrification, as was the case during the late SW monsoon 2007 between 250 and 400 m water depth (Gaye et al., 2013a).

Paleoceanographic studies from the Arabian Sea report the existence of a pronounced OMZ and elevated denitrification during interstadial (IS) and interglacial stages, whereas the Arabian Sea was well ventilated and denitrification was suppressed during stadials (Younger Dryas and Heinrich Events) and glacial stages (Altabet et al., 1995; Higginson et al., 2004; Möbius et al., 2011; Pichevin et al., 2007). Many studies used productivity proxies and SST reconstructions often in combination with denitrification proxies such as sedimentary $\delta^{15}N$ values to show that warm periods were characterized by a stronger SW monsoon inducing upwelling and higher productivity so that denitrification was switched on in the OMZ (Altabet et al., 1999, 2002; Pichevin et al., 2007; Reichart et al., 1997; Schulte et al., 1999; Suthhof et al., 2001). Many studies showed that monsoon fluctuations drove the past changes in ocean biogeochemistry (Böning and Bard, 2009; Clemens, 1998; Clemens and Prell, 2003; Deplazes et al., 2014; Pourmand et al., 2004).

After the transition from glacial to interglacial conditions with the warm and, respectively, cold excursions during the Bølling-Allerød and Younger Dryas, the Holocene was evidently a more stable period of permanent upwelling and denitrification (Böll et al., 2015; Overpeck et al., 1996; Pichevin et al., 2007; Tierney et al., 2016). There are, however, indications that millennial-scale climate oscillations similar to the North Atlantic cold periods detected by Bond et al. (1997), also occurred in the monsoon realm, however, with reduced amplitude. These Holocene cold periods were found to be characterized by reduced precipitation on land (Menzel et al., 2014) and reduced monsoonal upwelling in the Arabian Sea (Gupta et al., 2003). Volume and intensity of the mid-water OMZ appear to have oscillated related to SW monsoon strength, intensity of winter cooling by the NE monsoon as well as changes in OMZ ventilation (Böll et al., 2015; Das et al., 2017; Pichevin et al., 2007). Thus, understanding Holocene OMZ dynamics is indispensable to evaluate the recently observed OMZ intensification in the Arabian Sea (Banse et al., 2014; Rixen et al., 2014)

2.2 Sample collection

The two new cores included in this summary of SST and $\delta^{15}N$ records from the Arabian Sea are gravity core SL163 (21°55.97' N, 59°48.15' E, 650 m water depth) and multicore MC680 (22°37.16' N, 59°41.50' E, 789 m water depth). Both were retrieved in 2007 during Meteor cruise M74/1b from the continental margin off northern Oman. The first 400 cm of core 163SL were sampled in continuous 3 cm intervals and MC 680 was analyzed in 1 cm intervals. We analyzed alkenones in all sediment samples. $\delta^{15}N$ of MC680 was analyzed in

Biogeosciences Discuss., https://doi.org/10.5194/bg-2017-256
Manuscript under review for journal Biogeosciences
Discussion started: 27 June 2017

every second sample. All sediment samples were freeze-dried and homogenized prior to chemical treatment and analyses.

2.3 Analyses of the new cores 163 SL and MC680

Stable nitrogen isotopes

The ratio of the two stable isotopes of N ($^{15}N/^{14}N$) is expressed as $\delta^{15}N$, which is the per mil deviation from the N-isotope composition of atmospheric N_2 ($\delta^{15}N = 0$ ‰):

$$\delta^{15}N = [(R_{Sample}-R_{Standard})/R_{Standard}]*1000 \qquad (1)$$

where R_{Sample} is the $^{15}N/^{14}N$ ratio of the sample and $R_{Standard}$ is the $^{15}N/^{14}N$ ratio of atmospheric N_2. $\delta^{15}N$ values were determined using a Finnigan MAT 252 isotope ratio mass spectrometer after high-temperature flash combustion at 1100°C in a Carlo Erba NA-2500 elemental analyzer. Pure tank N_2 calibrated against the International Atomic Energy Agency reference standards IAEA-N-1 and IAEA-N-2, which were, in addition to an internal sediment standard, also used as working standards. Replicate measurements of a reference standard resulted in an analytical precision better than 0.2 ‰. The mean standard deviation based on duplicate measurements of samples is 0.07 ‰.

Alkenones

Sample preparation and detailed analytical procedure for alkenone identification are described in Böll et al. (2014). Purified lipid extracts of between 1.5 to 5 g freeze-dried and homogenized sediment samples were analyzed for alkenone concentrations using an Agilent 6850 gas chromatograph (GC) equipped with a split-splitless inlet system, a silica column (30 m x 0.25 µm film thickness x 0.32 mm ID; HP-1; Agilent) and a flame ionization detector

(310°C). Alkenone unsaturation ratios were translated into sea surface temperature using the core top calibration for the Indian Ocean of Sonzogni et al. (1997):

$$SST = (U^{K'}_{37} - 0.043)/0.033 \text{ with } U^{K'}_{37} = C_{37:2}/(C_{37:2} + C_{37:3}). \qquad (2)$$

All lipid extracts were analyzed twice resulting in a mean standard deviation of 0.2°C. The mean standard deviation of estimated SST based on replicate extraction and measurement of a working sediment standard is 0.5°C.

Age model

The age model for SL 163 was published by Munz et al. (2017). The age model of core MC680 is based on four accelerator mass spectrometry (AMS) ^{14}C datings from different core depths, measured at Beta Analytics, Miami/FL (see Table S1 and Figure F1 of supplementary information). Calibration and reservoir age correction were done in the same way as for 163SL (Munz et al., 2017). Both cores have a conspicuous sedimentation hiatus around 5700 years BP. In core MC680 the hiatus was positioned at 37 cm.

2.4 Integration and averaging of SST and $\delta^{15}N$ reconstructions

Temperature and $\delta^{15}N$ curves of most cores used here were taken from the literature (Table 1) except those for the new records of cores SL 163 and MC 680 presented for the first time in this paper (see above). All original data and all calculations are presented as Table S2 and S3 in the supplementary information.

In our compilation temperature reconstructions from the eastern Arabian Sea are based on Mg/Ca ratios of planktonic foraminifera (see methods in e.g. Govil and Naidu, 2010; Mahesh and Banakar, 2014; Saraswat et al., 2013; Tiwari et al., 2015). All other records are alkenone temperatures calculated with the core top calibration of Sonzogni et al. (1997b). Using the published age model, we averaged the temperature records available from the northern, western, eastern and southeastern Arabian Sea as well as for the Oman and Somali upwelling systems (Fig. 1b). Composites are based on two to five different core records. The data were binned in time slices of 1000 years for each individual sediment core. Next, all time slices of an age interval in a defined study area were averaged. The standard deviations of the calculated average SST curves rarely exceed the analytical precision of 0.5°C of alkenone based temperature reconstruction.

We are aware of the fact that alkenone and Mg/Ca derived SST may differ as proxies may be seasonally biased or impacted by dissolution or diagenesis (Huguet et al., 2006; Regenberg et al., 2014). Comparisons of different temperature proxies applied on the same core produced considerably different temperature estimates (Huguet et al., 2006; Munz et al., 2015). Mg/Ca and alkenone based temperatures are both calibrated with annual average temperatures from the surface layer (Regenberg et al., 2014; Sonzogni et al., 1997a; Sonzogni et al., 1997b) and may thus be comparable. Estimates of alkenone and Mg/Ca temperatures in core P178-15P from the Gulf of Aden were significantly correlated ($P < 0.05$) with a slope of 1 and an intercept of 0.5°C and had uniform trends (Tierney et al., 2016).

The average $\delta^{15}N$ values were calculated per time slice in a similar way as SST curves and averaged for the same areas (Fig. 1a). Before averaging the results of all curves of the selected areas, $\delta^{15}N$ values were normalized to an average value. The normalization procedure makes the relative changes in $\delta^{15}N$ comparable within each area despite differences in the diagenetic imprint and in $\delta^{15}N$ sources so that relative changes may be interpreted with respect to the relative intensity of denitrification. Average $\delta^{15}N$ curves of normalized values have a standard deviation of up to 1.5 ‰ with most values far below 1 ‰. The standard deviation is, generally, largest during deglaciation when $\delta^{15}N$ changed rapidly. The curves represent averages of four to seven individual curves except for Somali upwelling system where only

Biogeosciences Discuss., https://doi.org/10.5194/bg-2017-256
Manuscript under review for journal Biogeosciences
Discussion started: 27 June 2017

two curves were found. For the construction of the present $\delta^{15}N$ chart results from surface samples were included (Fig. 1a; Gaye-Haake et al., 2005).

3. Results

3.1 Temperature Reconstruction

All temperature reconstructions indicate lower SST during the Pleistocene compared to the Holocene (Fig. 3). Whereas SST in the southeastern region rise at about 20 ka BP in response to rising summer insolation over the northern hemisphere (Berger and Loutre, 1991), warming in the northern Arabian Sea and the upwelling areas started at about 17-16 ka BP, i.e. close to Termination 1 (Stern and Lisiecki, 2014). The largest SST increases from the Glacial to the Holocene can be observed in the northern (4°C) and the eastern (3°C) Arabian Sea. The increase in the Oman upwelling area is about 2.5°C and less than 2°C in the open western Arabian Sea, the Somali upwelling, and the southeastern Arabian Sea south of India. Some small scale temperature variabilities exceeding the analytical error of 0.5°C are visible. There is an increase of more than 1°C during the warm IS 2 in most regions except in the upwelling areas and the eastern equatorial Arabian Sea. SST minima during the Holocene occur at about 9 ka BP and 4-5 ka BP, respectively. The former is most prominent in the Oman and Somali upwelling areas and the latter in the northern and eastern Arabian Sea.

There is a change in the SST pattern in the basin between glacial conditions and the Holocene. During the last Glacial, the SST minimum was situated in the northern Arabian Sea and there is, generally, a north-south temperature increase (Fig. 4b). During the Holocene the SST pattern deviates from this north-south increase (Fig. 3; 4a): (i) SST in the Oman and Somali upwelling areas are lower than northern Arabian Sea temperatures, and (ii) SST in the eastern and southeastern Arabian Sea are in the same range.

3.2 Patterns of $\delta^{15}N$

The absolute $\delta^{15}N$ values in surface sediments in the present Arabian Sea are elevated with values between 6 and > 12 ‰ compared with those of the last Glacial with values between 3.5 and 7 ‰ (Fig. 5a, b). Holocene $\delta^{15}N$ values are highest in the central part of the basin and in the Oman upwelling area and lower in most shelf and slope sediments outside upwelling areas (Fig. 5a). Glacial shelf and slope sediments have $\delta^{15}N$ values below 6 ‰ and increase towards the center of the basin, similar to the present situation, but there are no glacial $\delta^{15}N$ records from the deepest part of the central Arabian Sea (Fig. 1a; 5b).

The $\delta^{15}N$ values increase between 16 and 14 ka BP in all sectors except in the eastern Arabian Sea, where the increase occurred at about 8 ka BP (Fig. 6). The normalized highest relative increase of $\delta^{15}N$ values by about 3.5 ‰ is observed in the northern Arabian Sea. All other normalized $\delta^{15}N$ curves increase by ≤ 2‰. Most integrated curves show a relative minimum during the Younger Dryas (11-12 ka BP) when $\delta^{15}N$ returned to the low glacial values. The Holocene $\delta^{15}N$ patterns differ across the basin. An early Holocene maximum is observed in the open western Arabian Sea, whereas a late Holocene maximum is visible in the northern and eastern part of the Arabian Sea. An early and late Holocene $\delta^{15}N$ peak occurs in the Oman and Somali upwelling areas.

4. Discussion

4.1. Temperature differences between Glacial and Holocene

The SST pattern in the modern Arabian Sea is strongly modulated by upwelling in the western part of the basin during the SW monsoon (Fig. 2a) and winter cooling in the northern Arabian Sea during the NE monsoon (Fig. 2b) as well as inflow of warm and low saline surface water from the Bay of Bengal via the North East Monsoon Current (NMC) and the West India

Coastal Current (WICC; Vijith et al., 2016). This inflow starts in the post SW-monsoon period probably forced by local winds around the southern tip of India (Suresh et al., 2016) and is related to prevailing sea level height difference between the Arabian Sea and Bay of Bengal which is due to the enhanced precipitation and river discharge to the Bay (Shankar and Shetye, 2001). The present annual average SST pattern is thus characterized by NW-SE oriented gradient (Fig. 4a). During the last Glacial the isotherms had a stronger latitudinal gradient indicating that the pattern was more insolation and less circulation driven (Fig. 4b). The main reason for this difference was a weakened SW and a strengthened NE monsoon so that upwelling was reduced or even inactive during the Glacial and the cold water source in the western Arabian Sea was shutdown (Duplessy, 1982). In addition, salinity reconstructions indicate that there was less advection of low salinity, warm surface waters into the eastern Arabian Sea from the Bay of Bengal probably due to the low glacial precipitation and river run-off (Mahesh and Banakar, 2014).

The temperature rise from the last Glacial to the Holocene in the near coastal regions of the Arabian Sea of 3-4°C is by 1-2°C larger than modelled for the tropical ocean (Annan and Hargreaves, 2013; Hopcroft and Valdes, 2015; Jansen et al., 2007). This may reflect much lower glacial land temperatures of central Asia (Annan and Hargreaves, 2013) which weakened the SW and strengthened the NE monsoon compared to the Holocene (Duplessy, 1982). Changes in annual average temperatures in the northern Arabian Sea were shown to be modulated mainly by the intensity of winter cooling and the resulting thermohaline mixing and thus added to the cooling induced by lower insolation during the Glacial (Böll et al., 2014; Böll et al., 2015; Reichart et al., 2004). A counter-clockwise surface circulation driven by a stronger NE monsoon advected these colder water masses to the northwestern part of the basin, adding to the cooling effect of convective winter cooling (Fig. 3b). Glacial SST is very similar off Somalia, in the open western and eastern Arabian Sea. Upwelling off Somalia and

Oman is driven by the positive wind stress curl induced by the Findlater Jet - a low level, cross equatorial jet stream, recurring during each SW monsoon over eastern Africa and the western Indian Ocean (Brock et al., 1991; Findlater, 1977). We assume that SW monsoonal upwelling was strongly reduced or inactive during cold phases of the Glacial and that the low temperatures off Oman are entirely related to convective overturn and advection of cold surface waters by the strong NE monsoon circulation.

The temperature gradients between the northern Arabian Sea on the one hand and the Oman and Somali upwelling areas on the other hand are a reflection of upwelling intensities and thus indicators of SW monsoon intensity (Böll et al., 2015). The strength of the Findlater Jet is directly coupled with the moisture transport to the Indian monsoon region (Fallah et al., 2016). Therefore, the strength of the SW monsoon is reflected by the index of effective moisture calculated from a large number of lake, peat, loess, and river records from the Asian continent by Herzschuh (2006). The increase of the moisture index coincides with strong increases in the upwelling indices between about 16 and 11 ka BP (Fig. 7). Peaks of the upwelling indices at 22-23 ka BP show that upwelling prevailed during IS2. During this short interglacial interval SST warmed and the upwelling was active for about two millennia. We do not observe a temperature minimum during the Younger Dryas (13-11.7 ka BP) in our averaged SST reconstructions (Fig. 3) but it is visible as a minimum of the upwelling indices at 12-13 ka BP (Fig. 7) and in SST records of high resolution (Böll et al., 2015; Huguet et al., 2006; Tierney et al., 2016). Due to the coarse resolution of most of our temperature curves this short cold excursion is obliterated during the steep temperature increase of deglaciation. A temperature minimum (Fig. 3) indicates strongest upwelling during the early Holocene climatic optimum (Böll et al., 2015). The second Holocene temperature minimum at around 4-5 ka BP cannot be observed in the central and southern part of the basin. It coincides with indications of climatic deterioration on the Indian peninsula (Prasad et al., 2014) as well as in other terrestrial climate records from Central Asia (Berkelhammer et al., 2012; Hong et al., 2003; Ponton et al., 2012) and may thus be due to a stronger NE monsoon with colder winters rather than to enhanced upwelling due to a warming event. The upwelling index follows the drop of the moisture index of the late Holocene with some delay (Fig. 7) while temperature records from the continent drop in parallel with the Asian moisture index (Herzschuh, 2006; Marcott et al., 2013; Peterse et al., 2014). We surmise that this either reflects a delayed response of the ocean or that higher summer temperatures due to reduced upwelling can to a certain extent, be compensated by lower winter temperatures.

4.2 Nitrogen cycling in the Glacial and Holocene

At present, nitrate reduction between 100-400 m water depths leaves residual nitrate with $\delta^{15}N$ values up to > 20 ‰ and upwelling can transport this enriched nitrate from 250-300 m water depth into surface waters in the western Arabian Sea upwelling areas (Gaye et al., 2013a; Yoshinari et al., 1997). Therefore, near shore sediments from the upwelling area off Oman have $\delta^{15}N$ elevated to > 10 ‰ (Fig. 5a). $\delta^{15}N$ values in all other recent sediments collected at water depths < 1000 m, i.e. at depths where the diagenetic effect on sedimentary $\delta^{15}N$ is small or negligible (Altabet and Francois, 1994; Gaye-Haake et al., 2005), are between 7 and 8 ‰. This is identical with the signal of sub-thermocline nitrate which feeds productivity primarily via seasonal deep mixing outside the upwelling areas (Gaye et al., 2013a; Gaye et al., 2013b). The $\delta^{15}N$ values >11 ‰ in the central part of the basin are a result of (i) offshore advection of ^{15}N enriched nitrate from upwelling areas where nitrate is not completely utilized (Naqvi et al., 2003), as well as (ii) early diagenetic increase of $\delta^{15}N$ in deep sea sediments (Gaye-Haake et al., 2005; Möbius et al., 2011).

Glacial $\delta^{15}N$ values from < 1000 m water depth are between 4 and 6 ‰ (Fig. 5b). This suggests that denitrification was very much reduced or absent, except during the IS when $\delta^{15}N$

values were elevated to almost Holocene levels (Möbius et al., 2011). OMZ sediments from the northern Arabian Sea were clearly bioturbated only during the stadials, i.e. the Younger Dryas and Heinrich Event, while they were indistinctly laminated during most of the last Glacial (Suthhof et al., 2001). This indicates that suboxic conditions prevailed during the Glacial in the northern Arabian Sea so that bioturbation was reduced. $\delta^{15}N$ records of the last 60 ka suggest that the Arabian Sea rapidly oscillated between denitrification during the short IS time intervals and no denitrification under normal glacial conditions and during Heinrich events and stadials (Altabet et al., 1995; Suthhof et al., 2001). Glacial conditions in the Arabian Sea thus may have been comparable to those in the present Bay of Bengal, where nitrate reduction and denitrification occur locally at a low level, but the enriched nitrate is not transported into surface waters (Bristow et al., 2017). The glacial Arabian Sea quickly switched to enhanced denitrification when the SW-monsoon strengthened, so that upwelling induced productivity rose and oxygen concentrations in the OMZ sank below the threshold for denitrification of 4-5 µM O_2. Upwelling was, furthermore, an effective process to transport the denitrification signal into the surface waters, so that it was recorded in the underlying sediments.

Enhanced N fixation has been suggested as an alternative reason for the low $\delta^{15}N$ in glacial sediment intervals from the Arabian Sea (Altabet et al., 1995; Emeis et al., 1995; Suthhof et al., 2001), stimulated by the supply of excess phosphate and iron from the more arid continents via dust supply (Prins, 1999; Sirocko et al., 2000). In this case, N fixation in surface waters provided N with low $\delta^{15}N$ that may have masked the high $\delta^{15}N$ signal from denitrification. Glacial OMZ ventilation was more dominated by the inflow of IOCW which could prograde deeper into the northern part of the basin as the lower sea level severely reduced the inflow of PGW and RSW (Pichevin et al., 2007, Rixen and Ittekkot, 2005). Deep mixing probably added to ventilation of the upper OMZ during stadials in the northern

Arabian Sea (Reichart et al., 2004) so that denitrification was significant only when productivity became enhanced and ventilation reduced during IS (Pichevin et al., 2007).

The steep increase of $\delta^{15}N$ values starts at 14-15 ka BP, almost simultaneously with the SST increase in most parts of the basin except for the eastern Arabian Sea (Fig. 6). This shows that denitrification was enhanced immediately when the SW monsoon and thus monsoonal upwelling strengthened. This implies that enhanced productivity and particle flux triggered denitrification in the OMZ almost in the entire basin. A short return to glacial conditions without denitrification across the basin occurred during the cold excursion of the Younger Dryas. The $\delta^{15}N$ minimum between 9 to 5 ka BP is most prominent in the Oman upwelling area and is probably a signal of enhanced early and mid-Holocene OMZ ventilation. Benthic foraminifera indicate that oxygen concentrations were high and denitrification was low during this period (Das et al., 2017) despite enhanced upwelling as indicated by the low SST (see above) and enhanced productivity (Das et al., 2017). Evidently, the vigorous upwelling during the Holocene climatic optimum was fed by inflow of IOCW from the south which ventilated the western Arabian Sea and thus compensated for the enhanced respiration (Rixen et al., 2014).

Denitrification has continuously increased during the Holocene in almost the entire basin but focused in the northern Arabian Sea (Fig. 6b). This trend coincides with Holocene cooling and a strengthening of the NE monsoon. Only in the western Arabian Sea outside direct upwelling influence, $\delta^{15}N$ values decrease in the late Holocene (Fig. 6d), but this may be related to the reduced advection of ^{15}N enriched nitrate from the adjacent upwelling areas. Pichevin et al. (2007) pointed out that circulation probably changed after the sea level in the Persian Gulf and Red Sea reached its present position at about 6 ka BP and water masses from these two basins prevented the ingression of IOCW to the north-eastern part of the Arabian Sea. The ventilation of the OMZ by PGW and RSW today is restricted to the western part of the basin where at present the OMZ is much weaker than in the eastern and northeastern part of the basin (Gaye et al., 2013a). PGW and RSW are, furthermore, more depleted in oxygen than the inflowing IOCW. The interplay of reduced OMZ ventilation and enhanced NE monsoon productivity are likely reasons for the relocation of the OMZ and denitrification maximum to the NE part of the basin during the Holocene. Enhanced productivity in the eastern Arabian Sea as reconstructed from sediment cores (Agnihotri et al., 2003; Kessarkar et al., 2013; Kessarkar et al., 2010) added to this relocation. After precipitation declined and the sea level difference between the Bay of Bengal and Arabian Sea dropped at about 8 ka BP (Mahesh and Banakar, 2014), the inflow of warm low saline water with the northeast monsoon current and WICC to the eastern Arabian Sea declined. This is coinciding with a rise in eastern Arabian Sea $\delta^{15}N$ (Fig. 6c). It is likely that this inflow of low density surface water suppressed primary productivity in the eastern Arabian Sea in the early Holocene. Today, the OMZ is, constrained to the SE by a northward undercurrent which leads to oxygenation of subsurface water (Resplandy et al., 2012) and its upwelling along the coast is likely to explain the low $\delta^{15}N$ in the sediments off the SE coast of India (Fig. 5a).

Total organic carbon mass accumulation rates (TOC MAR; Fig. 6g) reflect productivity, organic matter preservation and burial efficiency (Cowie et al., 2014; Cowie and Hedges, 1993; Müller and Suess, 1979). Similar to $\delta^{15}N$, Arabian Sea TOC MAR deviates from the global pattern compiled by Cartapanis et al. (2016). Whereas the global TOC MAR significantly declines during deglaciation and remains low throughout the Holocene, the TOC MAR of the Arabian Sea are relatively low only between about 10-15 ka BP (Fig. 6g). This trend is, however, curtailed by the large standard deviation throughout the record from the Arabian Sea (Fig. 6g). The drop during deglaciation may indicate a reduction of both, productivity and burial efficiency of TOC in sediments. Both could be spawned by reduced dust supply which may have induced iron limitation so that N fixation was reduced. Iron

Biogeosciences Discuss., https://doi.org/10.5194/bg-2017-256
Manuscript under review for journal Biogeosciences
Discussion started: 27 June 2017

limitation has been suggested to reduce N fixation worldwide after the LGM and therewith the oceanic N inventory may have decreased drastically (Eugster et al., 2013). The strong early Holocene upwelling and late Holocene NE monsoon strengthening may have facilitated the higher Holocene TOC MAR compared to deglaciation in the Arabian Sea. However, the increase of TOC MAR from the early to the late Holocene may as well be due to better preservation caused by progressive deoxygenation (Cowie et al., 2014; Paropkari et al., 1995).

Results from a global climate and ocean biogeochemistry model (KCM/PISCES; Aumont et al., 2003; Park and Latif, 2008) driven by astronomical forcing over the Holocene suggest that ventilation changes were important drivers of the late Holocene Arabian Sea OMZ intensification (Fig. 8). The model produces a continuous increase of the OMZ volume in the Arabian Sea from 10 ka BP to the present. This is driven mainly by an increasing age (time since contact with the surface) of the water masses in the Arabian Sea OMZ. Arabian Sea export production is fairly constant in the model (Figure 8) and can thus be ruled out as the driver for deoxygenation. An increase in export production is modelled only in a small area west of the Southern Indian coast, indicating that export changes may only have played a local role (not shown). The decelerated circulation allowed more oxygen to be consumed by remineralization, and thus appears to be the main driver of the progressive deoxygenation in the model (Fig. 8) and can explain the increasing water column denitrification in the Arabian Sea in the $\delta^{15}N$ records (Fig. 6).

5. Summary and Conclusions

Glacial ocean surface circulation in the Arabian Sea was generally reduced compared to Holocene circulation. Monsoonal upwelling along the western coasts was very much reduced or absent, as was inflow of warm equatorial water and low salinity water from the Bay of Bengal. Therefore, the general temperature gradient had a stronger insolation-driven N-S trend compared to the circulation-driven NE-SW trend of the Holocene. Pronounced convective mixing caused by a strong NE monsoon added to the insolation-related low temperatures so that SST in the northern Arabian Sea was 4°C colder than Holocene temperatures. The difference between northern Arabian Sea temperatures and temperatures from the Oman and Somali upwelling areas is an upwelling indicator, as SST in the upwelling areas drop below those of the northern Arabian Sea. According to this index, upwelling was active during the warm IS as well as during the entire Holocene with a maximum between 6-10 ka BP. Upwelling increased in concert with the effective moisture over Asia at 16 ka BP (Herzschuh, 2006) both driven by the SW monsoon strength.

Glacial $\delta^{15}N$ values in slope sediments were by 2-5 ‰ lower than Holocene $\delta^{15}N$ and indicate that denitrification was significantly reduced or absent in the glacial Arabian Sea and that the OMZ was much less intense. In analogy to conditions in the recent Bay of Bengal, $\delta^{15}N$ of 4-6 ‰ in glacial sediments may not necessarily indicate that denitrification was completely absent. Moderate or occasional denitrification may have taken place in a more oxygenated OMZ, but its $\delta^{15}N$ signal was not recorded in the sediment because the sub-thermocline water mass was isolated from the euphotic zone by stratification. Also, atmospheric N sources (eolian supply or N_2 fixation) contributed to the low $\delta^{15}N$ of 4-5 ‰ and compensated the enhanced $\delta^{15}N$ in the OMZ. The stronger NE monsoon may have added to a seasonal erosion of the OMZ via deep convective overturning (Reichart et al., 2004). We surmise that the system could quickly respond to changes in productivity. It shifted from low to strong denitrification during the short warm IS interplays as upwelling and thus productivity increased. Oxygenation prevailed during the Younger Dryas and Heinrich Events as the nutrient supply to surface waters was at its glacial minimum (Schmittner et al., 2007). Simultaneous with the indication of first upwelling at about 15 ka BP, $\delta^{15}N$ values increased significantly but indicate almost glacial conditions for a short interval during the Younger

Dryas. After this, oceanic circulation increased ventilation especially during the period of most vigorous upwelling in the early to mid-Holocene (Das et al., 2017). The mid-Holocene sea level rise and enhanced inflow of RSW and PGW probably obstructed the ventilation of the northern Arabian Sea (Das et al. 2017; Pichevin et al., 2007). The present OMZ pattern with the denitrification maximum in the northeastern part of the basin was probably formed after 4-5 ka BP and may additionally be augmented by enhanced productivity in the northern and eastern Arabian Sea due to the strengthened NE monsoon and reduced inflow of low saline water from the Bay of Bengal after the Holocene climatic optimum. However, the KCM/PISCES model simulation suggests that the main driver of increasing deoxygenation and denitrification in the Arabian Sea is the prolonged residence time of OMZ waters.

Acknowledgements

We are grateful to the German Federal Ministry of Education and Research (BMBF) for funding the BMBF projects CARIMA and CAHOL as subprojects of the research programmes CAME and, respectively, CAME II (BMBF grants 03G0806A, 03G0806B, 03G0806C, 030864A). We thank F. Langenberg and S. Beckmann for analytical support. Reiner Schlitzer and the ODV group are acknowledged for supplying the program Ocean Data View.

References

Agnihotri, R., Bhattacharya, S. K., Sarin, M. M., and Somayajulu, B. L. K.: Changes in surface productivity and subsurface denitrification during the Holocene: a multiproxy study from the eastern Arabian Sea, The Holocene, 13, 701-713, 2003.

Agnihotri, R., Kurian, S., Fernandes, M., Reshma, K., D'Souza, W., and Naqvi, S. W. A.: Variability of subsurface denitrification and surface productivity in the coastal eastern Arabian Sea over the past seven centuries, Holocene, 18, 755-764, 2008.

Altabet, M., Francois, R., Murray, D., and Prell, W.: Climate-related variations in denitrification in the Arabian Sea from sediment $^{15}N/^{14}N$ ratios, Nature, 373, 506-509, 1995.

Altabet, M. A. and Francois, R.: Sedimentary nitrogen isotopic ratio as a recorder of surface ocean nitrate utilization, Global Biogeochemical Cycles, 8, 103-116, 1994.

Altabet, M. A., Higginson, M. J., and Murray, D. W.: The effect of millennial-scale changes in Arabian Sea denitrification on atmospheric CO_2, Nature, 415, 159-162, 2002.

Annan, J. D. and Hargreaves, J. C.: A new global reconstruction of temperature changes at the Last Glacial Maximum, Clim. Past, 9, 367-376, 2013.Aumont, O., Maier-Reimer, E., Blain, S., and Monfray, P.: An ecosystem model of the global ocean including Fe, Si, P colimitations, Global Biogeochemical Cycles, 17, 26, 2003.

Banakar, V. K., Mahesh, B. S., Burr, G., and Chodankar, A. R.: Climatology of the Eastern Arabian Sea during the last glacial cycle reconstructed from paired measurement of foraminiferal delta O-18 and Mg/Ca, Quaternary Research, 73, 535-540, 2010.

Banse, K., Naqvi, S. W. A., Narvekar, P. V., Postel, J. R., and Jayakumar, D. A.: Oxygen minimum zone of the open Arabian Sea: variability of oxygen and nitrite from daily to decadal timescales, Biogeosciences, 11, 2237-2261, 2014.

Bard, E., Rostek, F., and Sonzogni, C.: Interhemispheric synchrony of the last deglaciation inferred from alkenone palaeothermometry, Nature, 385, 707-710, 1997.

Berger, A. and Loutre, M. F.: Insolation values for the climate of the last 10 million years, Quaternary Science Reviews, 10, 297-317, 1991.

Berkelhammer, M., Sinha, A., Stott, L., Cheng, H., Pausata, F. S. R., and Yoshimura, K.: An Abrupt Shift in the Indian Monsoon 4000 Years Ago. In: Climates, Landscapes, and Civilizations, Giosan, L., Fuller, D. Q., Nicoll, K., Flad, R. K., and Clift, P. D. (Eds.), Geophysical Monograph Series, pp. 75-87, Amer Geophysical Union, Washington, 2012.

Böll, A., Lückge, A., Munz, P., Forke, S., Schulz, H., Ramaswamy, V., Rixen, T., Gaye, B., and Emeis, K.-C.: Late Holocene primary productivity and sea surface temperature variations in the northeastern Arabian Sea: Implications for winter monsoon variability, Paleoceanography, 29, 778-794; 2013PA002579, 2014.

Böll, A., Schulz, H., Munz, P., Rixen, T., Gaye, B., and Emeis, K.-C.: Contrasting sea surface temperature of summer and winter monsoon variability in the northern Arabian Sea over the last 25ka, Palaeogeography, Palaeoclimatology, Palaeoecology, 426, 10-21, 2015.

Bond, G., Showers, W., Cheseby, M., Lotti, R., Almasi, P., deMenocal, P. B., Priore, P., Cullen, H. M., Hajdas, I., and Bonani, G.: A pervasive millenial-scale cycle in North Atlantic Holocene and Glacial Climates, Science, 278, 1257-1266, 1997.

Böning, P. and Bard, E.: Millenial/centennial-scale thermocline ventilation changes in the Indian Ocean as reflected by aragonite preservation and geochemical variations in the Arabian Sea sediments, Geochimica et Cosmochimica Acta, 73, 6771-6788, 2009.

Brandes, J. A. and Devol, A. H.: A global marine-fixed nitrogen isotopic budget: Implications for Holocene nitrogen cycling, Global Biogeochemical Cycles, 16, 10.1029/2001GB001856, 2002.

Brandes, J. A., Devol, A. H., Yoshinari, T., Jayakumar, D. A., and Naqvi, S. W. A.: Isotopic composition of nitrate in the central Arabian Sea and eastern tropical North Pacific: A

Biogeosciences Discuss., https://doi.org/10.5194/bg-2017-256
Manuscript under review for journal Biogeosciences
Discussion started: 27 June 2017

tracer for mixing and nitrogen cycles, Limnology and Oceanography, 43, 1680-1689, 1998.

Bristow, L. A., Callbeck, C. M., Larsen, M., Altabet, M. A., Dekaezemacker, J., Forth, M., Gauns, M., Glud, R. N., Kuypers, M. M. M., Lavik, G., Milucka, J., Naqvi, S. W. A., Pratihary, A., Revsbech, N. P., Thamdrup, B., Treusch, A. H., and Canfield, D. E.: N2 production rates limited by nitrite availability in the Bay of Bengal oxygen minimum zone, Nature Geoscience, 10, 24-29, doi:10.1038/ngeo2847, 2017.

Brock, J. C., McClain, C. R., Luther, M. E., and Hay, W. W.: The phytoplankton bloom in the northwestern Arabian Sea during the southwest monsoon of 1979, Journal of Geophysical Research-Oceans, 96, 20623-20642, 1991.

Budziak, D.: Alkenones of sediment core GeoB3007-3. In: In: Budziak, D (2001): Alkenone analyses of sediment cores from the western Arabian Sea. doi:10.1594/PANGAEA.804466, PANGAEA, 2004.

Carpenter, E., Harvey, H., Fry, B., and Capone, D.: Biogeochemical tracers of the marine cyanobacterium Trichodesmium, Deep-Sea Research I, 44, 27-38, 1997.

Cartapanis, O., Bianchi, D., Jaccard, S. L., and Galbraith, E. D.: Global pulses of organic carbon burial in deep-sea sediments during glacial maxima, Nature Communications, 7, 10796, 2016.

Clemens, S. C.: Dust response to seasonal atmospheric forcing: proxy evaluation and calibration, Paleoceanography, 13, 471-490, 1998.

Clemens, S. C. and Prell, W. L.: A 350,000 year summer-monsoon multi-proxy stack from the Owen Ridge, Northern Arabian Sea, Marine Geology, 201, 35-51, 2003.

Cline, J. D. and Kaplan, I. R.: Isotopic fractionation of dissolved nitrate during denitrification in the eastern tropical North Pacific, Marine Chemistry, 3, 271-299, 1975.

Codispoti, L. A.: An oceanic fixed nitrogen sink exceeding 400 Tg N a^{-1} vs the concept of homeostasis in the fixed-nitrogen budget, Biogeosciences, 4, 233-253, 2007.

Codispoti, L. A., Brandes, J. A., Christensen, J. P., Devol, A. H., Naqvi, S. W. A., Pearl, H. W., and Yoshinari, T.: The oceanic fixed nitrogen and nitrous oxide budgets: Moving targets as we enter the anthropocene?, Scientia Marina, 65, 85-105, 2001.

Cowie, G., Mowbray, S., Kurian, S., Sarkar, A., White, C., Anderson, A., Vergnaud, B., Johnstone, G., Brear, S., Woulds, C., Naqvi, S. W. A., and Kitazato, H.: Comparative organic geochemistry of Indian margin (Arabian Sea) sediments: estuary to continental slope, Biogeosciences, 11, 6683-6696, 2014.

Cowie, G. L. and Hedges, J. I.: A comparison of organic matter sources, diagenesis and preservation in oxic and anoxic coastal sites, Chemical Geology, 107, 447-451, 1993.

Das, M., Singh, R. K., Gupta, A. K., and Bhaumik, A. K.: Holocene strengthening of the Oxygen Minimum Zone in the northwestern Arabian Sea linked to changes in intermediate water circulation or Indian monsoon intensity?, Palaeogeography, Palaeoclimatology, Palaeoecology, doi: http://dx.doi.org/10.1016/j.palaeo.2016.10.035, 2017.

Deplazes, G., Lückge, A., Stuut, J.-B. W., Pätzold, J., Kuhlmann, H., Husson, D., Fant, M., and Haug, G. H.: Weakening and strengthening of the Indian monsoon during Heinrich events and Dansgaard-Oeschger oscillations, Paleoceanography, 29, 2013PA002509, 2014.

Deutsch, C., Sigman, D. M., Thunell, R. C., Meckler, A. N., and Haug, G. H.: Isotopic constraints on glacial/interglacial changes in the oceanic nitrogen budget, Global Biogeochemical Cycles, 18, GB4012, doi:4010.1029/2003GB002189, 2004.

DeVries, T., Deutsch, C., Rafter, P. A., and Primeau, F.: Marine denitrification rates determined from a global 3-D inverse model, Biogeosciences, 10, 2481-2496, 2013.

Duplessy, J. C.: Glacial to interglacial contrast in the northern Indian Ocean, Nature, 295, 494-498, 1982.

Emeis, K.-C., Anderson, D. M., Doose, H., Kroon, D., and Schulz-Bull, D.: Sea-Surface Temperatures and the History of Monsoon Upwelling in the Northwest Arabian Sea during the Last 500,000 Years, Quaternary Research, 43, 355-361, 1995.

Eugster, O., Gruber, N., Deutsch, C., Jaccard, S. L., and Payne, M. R.: The dynamics of the marine nitrogen cycle across the last deglaciation, Paleoceanography, 28, 14, 2013.

Fallah, B., Cubasch, U., Prömmel, K., and Sodoudi, S.: A numerical model study on the behaviour of Asian summer monsoon and AMOC due to orographic forcing of Tibetan Plateau, Climate Dynamics, 47, 1485-1495, 2016.

Findlater, J.: Observational aspects of the low-level cross-equatorial jet stream of the western Indian Ocean. Pure Applied Geophysics, 115, 1251-1262, 1977.

Galbraith, E. D., Kienast, M., Albuquerque, A. L., Altabet, M. A., Batista, F., Bianchi, D., Calvert, S. E., Contreras, S., Crosta, X., De Pol-Holz, R., Dubois, N., Etourneau, J., Francois, R., Hsu, T. C., Ivanochko, T., Jaccard, S. L., Kao, S. J., Kiefer, T., Kienast, S., Lehmann, M. F., Martinez, P., McCarthy, M., Meckler, A. N., Mix, A., Mobius, J., Pedersen, T. F., Pichevin, L., Quan, T. M., Robinson, R. S., Ryabenko, E., Schmittner, A., Schneider, R., Schneider-Mor, A., Shigemitsu, M., Sinclair, D., Somes, C., Studer, A. S., Tesdal, J. E., Thunell, R., Yang, J. Y. T., and Members, N. W. G.: The acceleration of oceanic denitrification during deglacial warming, Nature Geoscience, 6, 579-584, 2013.

Ganeshram, R. S., Pedersen, T. F., Calvert, S. E., McNeill, G. W., and Fontugne, M. R.: Glacial-interglacial variability in denitrification in the world's oceans: Causes and consequences, Paleoceanography, 15, 361-376, 2000.

Ganeshram, R. S., Pedersen, T. F., Calvert, S. E., and Murray, J. W.: Large changes in oceanic nutrient inventories from glacial to interglacial periods. Nature, 376, 755-758, 1995.

Gaye-Haake, B., Lahajnar, N., Emeis, K.-C., Unger, D., Rixen, T., Suthhof, A., Ramaswamy, V., Schulz, H., Paropkari, A. L., Guptha, M. V. S., and Ittekkot, V.: Stable nitrogen isotopic ratios of sinking particles and sediments from the northern Indian Ocean, Marine Chemistry, 96, 243-255, 2005.

Gaye, B., Nagel, B., Dähnke, K., Rixen, T., and Emeis, K. C.: Evidence of parallel denitrification and nitrite oxidation in the ODZ of the Arabian Sea from paired stable isotopes of nitrate and nitrite Global Biogeochemical Cycles, 27, doi10.1002/2011GB004115, 2013a.

Gaye, B., Nagel, B., Dähnke, K., Rixen, T., Lahajnar, N., and Emeis, K. C.: Amino acid composition and $\delta^{15}N$ of suspended matter in the Arabian Sea: implications for organic matter sources and degradation, Biogeosciences 10, 7689-7702, 2013b.

Govil, P. and Naidu, P. D.: Evaporation-precipitation changes in the eastern Arabian Sea for the last 68 ka: Implications on monsoon variability, Paleoceanography, 25, 11, 2010.

Grootes, P. M. and Stuiver, M.: Oxygen 18/16 variability in Greenland snow and ice with 10^{-3}- to 10^{5}-year time resolution, Journal of Geophysical Research: Oceans, 102, 26455-26470, 1997.

Grosskopf, T., Mohr, W., Baustian, T., Schunck, H., Gill, D., Kuypers, M. M. M., Lavik, G., Schmitz, R. A., Wallace, D. W. R., and LaRoche, J.: Doubling of marine dinitrogen-fixation rates based on direct measurements, Nature, 488, 361-364, 2012.

Gruber, N.: The marine nitrogen cycle: Overview and challenges. In: Nitrogen in the Marine Environment, 2nd Edition, Capone, D. G., Bronk, D. A., Mulholland, M. R., and Carpenter, E. (Eds.), 51 p., Academic Press, San Diego, 2008.

Gruber, N. and Galloway, J. N.: An earth-system perspective of the global nitrogen cycle, Nature, 451, 293-296, 2008.

Gruber, N. and Sarmiento, J. L.: Global patterns of marine nitrogen fixation and denitrification, Global Biogeochemical Cycles, 11, 235-266, 1997.

Gupta, A. K., Anderson, D. M., and Overpeck, J. T.: Abrupt changes in the Asian southwest monsoon during the Holocene and their links to the North Atlantic Ocean, Nature, 421, 354-357, 2003.

Herzschuh, U.: Palaeo-moisture evolution in monsoonal Central Asia during the last 50,000 years, Quaternary Science Reviews, 25, 163-178, 2006.

Higginson, M. J., Altabet, M. A., Murray, D. W., Murray, R. W., and Herbert, T. D.: Geochemical evidence for abrupt changes in relative strength of the Arabian monsoons during a stadial/interstadial climate transition, Geochimica et Cosmochimca Acta, 68, 3807-3826, 2004.

Hong, Y. T., Hong, B., Lin, Q. H., Zhu, Y. X., Shibata, Y., Hirota, M., Uchida, M., Leng, X. T., Jiang, H. B., Xu, H., Wang, H., and Yi, L.: Correlation between Indian Ocean summer monsoon and North Atlantic climate during the Holocene, Earth and Planetary Science Letters, 211, 371-380, 2003.

Hopcroft, P. O. and Valdes, P. J.: How well do simulated last glacial maximum tropical temperatures constrain equilibrium climate sensitivity?, Geophysical Research Letters, 42, 5533-5539, 2015.

Huguet, C., Kim, J.-H., Sinninghe Damsté, J. S., and Schouten, S.: Reconstruction of sea surface temperature variations in the Arabian Sea over the last 23 kyr using organic proxies (TEX86 and U37K′), Paleoceanography, 21, PA3003, 2006.

Isaji, Y., Kawahata, H., Ohkouchi, N., Ogawa, N. O., Murayama, M., Inoue, K., and Tamaki, K.: Varying responses to Indian monsoons during the past 220 kyr recorded in deep-sea sediments in inner and outer regions of the Gulf of Aden, Journal of Geophysical Research-Oceans, 120, 7253-7270, 2015.

Ivanochko, T. S., Ganeshram, R. S., Brummer, G.-J. A., Ganssen, G., Jung, S. J. A., Moreton, S. G., and Kroon, D.: Variations in tropical convection as an amplifier of global climate change at the millennial scale, Earth and Planetary Science Letters, 235, 302-314, 2005.

Jansen, E., Overpeck, J., Briffa, K. R., Duplessy, J.-C., Joos, F., Masson-Delmotte, V., Olago, D., Otto-Bliesner, B., Peltier, W. R., Rahmstorf, S., Ramesh, R., Raynaud, D., Rind, D., Solomina, O., R., V., and Zhang, D.: Paleoclimate. In: Climate Change 2007: The Physical Science Basis. Contribution of Working Group I to the Fourth Assessment Report of the Intergovernmental Panel on Climate Change Solomon, S., Qin, D., Manning, M., Chen, Z., Marquis, M., Averyt, K. B., M., T., and Miller, H. L. M. (Eds.), Cambridge University Press, Cambridge, United Kingdom and New York, NY, USA, 2007.

Jaeschke, A., Ziegler, M., Hopmanns, E. C., Reichart, G. J., Lourens, L. J., Schouten, S., and Sinninghe Damsté, J. S.: Molecular fossil evidence for anaerobic ammonium oxidation in the Arabian Sea over the last glacial cycle, Paleoceanography, 24, doi:10.1029/2008PA001712, 2009.

Jensen, M. M., Lam, P., Revsbech, N. P., Nagel, B., Gaye, B., Jetten, M. S. M., and Kuypers, M. M. M.: Intensive nitrogen loss over the Omani shelf due to anammox coupled with dissimilatory nitrite reduction to ammonium, The International Society for Microbial Ecology Journal, 5, 1660-1670; doi:1610.1038/ismej.2011.1644, 2011.

Kessarkar, P. M., Purnachadra Rao, V., Naqvi, S. W. A., and Karapurkar, S. G.: Variation in the Indian summer monsoon intensity during the Bølling-Ållerød and Holocene, Paleoceanography, 28, 413-425, 2013.

Kessarkar, P. M., Rao, V. P., Naqvi, S. W. A., Chivas, A. R., and Saino, T.: Fluctuations in productivity and denitrification in the southeastern Arabian Sea during the Late Quaternary, Current Science, 99, 485-491, 2010.

Mahesh, B. S. and Banakar, V. K.: Change in the intensity of low-salinity water inflow from the Bay of Bengal into the Eastern Arabian Sea from the Last Glacial Maximum to the Holocene: Implications for monsoon variations, Palaeogeography,. Palaeoclimatolology, Palaeoecology, 397, 31-37, 2014.

Marcott, S. A., Shakun, J. D., Clark, P. U., and Mix, A. C.: A Reconstruction of Regional and Global Temperature for the Past 11,300 Years. , Science, 339, 1198, 2013.

Menzel, P., Gaye, B., Mishra, P. K., Anoop, A., Basavaiah, N., Marwan, N., Plessen, B., Prasad, S., Riedel, N., Stebich, M., and Wiesner, M. G.: Linking Holocene drying trends from Lonar Lake in monsoonal central India to North Atlantic cooling events, Palaeogeography, Palaeoclimatology, Palaeoecology, 410, 164-178, 2014.

Möbius, J., Gaye, B., Lahajnar, N., Bahlmann, E., and Emeis, K.-C.: Influence of diagenesis on sedimentary $\delta^{15}N$ in the Arabian Sea over the last 130 kyr, Marine Geology, 284, 127-138; doi: 110.1016/j.margeo.2011.1003.1013, 2011.

Müller, P. J. and Suess, E.: Productivity, sedimentation rate, and sedimentary organic matter in the oceans-I. Organic carbon preservation, Deep-Sea Research, 26A, 1347-1362, 1979.

Munz, P. M., Siccha, M., Lückge, A., Boll, A., Kucera, M., and Schulz, H.: Decadal-resolution record of winter monsoon intensity over the last two millennia from planktic foraminiferal assemblages in the northeastern Arabian Sea, Holocene, 25, 1756-1771, 2015.

Munz, P. M., Steinke, S., Böll, A., Lückge, A., Groeneveld, J., Kucera, M., and Schulz, H.: Decadal resolution record of Oman margin upwelling indicates persistent solar forcing of the Indian summer monsoon after the early Holocene summer insolation maximum, Climate of the Past 13, 491-509, 2017.

Naqvi, S. W. A., Naik, H., and Narvekar, P. V.: The Arabian Sea. In: Biogeochemistry in Marine Systems, Black, K. and Shimmield, G. (Eds.), Academic Press, Sheffield, 2003.

Naqvi, S. W. A., Noronha, R. J., Somasundar, K., and Sen Gupta, R.: Seasonal changes in the denitrification regime of the Arabian Sea, Deep-Sea Research, 37, 593-611, 1990.

Overpeck, J., Anderson, D., Trumbore, S., and Prell, W.: The southwest Indian Monsoon over the last 18,000 years, Climate. Dynamics, 12, 213-225, 1996.

Park, W. and Latif, M.: Multidecadal and multicentennial variability of the meridional overturning circulation, Geophysical Research Letters, 35, 5, 2008.

Paropkari, A. L., Prakash Babu, C., and Mascarenas, A.: New evidence for enhanced preservation of organic carbon in contact with oxygen minimum zone on the western continental slope of India, Marine Geology, 111, 7-13, 1995.

Peterse, F., Martínez-García, A., Zhou, B., Beets, C. J., Prins, M. A., Zheng, H., and Eglinton, T. I.: Molecular records of continental air temperature and monsoon precipitation variability in East Asia spanning the past 130,000 years, Quaternary Science Reviews, 83, 76-82, 2014.

Pichevin, L., Bard, E., Martinez, P., and Billy, I.: Evidence of ventilation changes in the Arabian Sea during the late Quaternary: Implication for denitrification and nitrous oxide emission, Global Biogeochemical Cycles, 21, GB4008, doi:4010.1029/2006GB002852, 2007.

Ponton, C., Giosan, L., Eglinton, G., Fuller, D. Q., Johnson, J. E., Kumar, P. S., and Collett, T. S.: Holocene aridification of India, Geophysical Research Letters, 39, 10.1029/2011GL050722, 2012.

Biogeosciences Discuss., https://doi.org/10.5194/bg-2017-256
Manuscript under review for journal Biogeosciences
Discussion started: 27 June 2017

Biogeosciences
Discussions
Open Access
EGU

Pourmand, A., Marcantonio, F., Bianchi, T. S., Canuel, E. A., and Waterson, E. J.: A 28-ka history of sea surface temperature, primary productivity and planktonic community variability in the western Arabian Sea, Paleoceanography, 22, 1-14, 2007.

Pourmand, A., Marcantonio, F., and Schulz, H.: Variations in productivity and eolian fluxes in the northeastern Arabian Sea during the past 110 ka, Earth and Planetary Science Letters, 221, 39-54, 2004.

Prasad, S., Anoop, A., Riedel, N., Sarkar, S., Menzel, P., Basavaiah, N., Krishnan, R., Fuller, D., Plessen, B., Gaye, B., Röhl, U., Wilkes, H., Sachse, D., Sawant, R., Wiesner, M. G., and Stebich, M.: Prolonged monsoon droughts and links to Indo-Pacific warm pool: A Holocene record from Lonar Lake, central India, Earth and Planetary Science Letters, 391, 171-182, 2014.

Prins, M. A.: Pelagic, hemipelagic and turbidite deposition iin the Arabian Sea during the Late Quaternary, Geologica Ultraiectina, 168, 192, 1999.

Regenberg, M., Regenberg, A., Garbe-Schonberg, D., and Lea, D. W.: Global dissolution effects on planktonic foraminiferal Mg/Ca ratios controlled by the calcite-saturation state of bottom waters, Paleoceanography, 29, 127-142, 2014.

Reichart, G. J., Brinkhuis, H., Huiskamp, F., and Zachariasse, W. J.: Hyperstratification following glacial overturning events in the northern Arabian Sea, Paleoceanography, 19, 8, 2004.

Reichart, G. J., Lourens, L. J., and Zchariasse, W. J.: Temporal variability in the northern Arabian Sea oxygen minimum zone (OMZ) during the last 225,000 years, Paleoceanography, 13, 607-621, 1998.

Ren, H. J., Sigman, D. M., Chen, M. T., and Kao, S. J.: Elevated foraminifera-bound N isotopic composition during the last ice age in the South China Sea and its global and regional implications, Global Biogeochemical Cycles, 26, 13, 2012.

Resplandy, L., Levy, M., Bopp, L., Echevin, V., Pous, S., Sarma, V., and Kumar, D.: Controlling factors of the oxygen balance in the Arabian Sea's OMZ, Biogeosciences, 9, 5095-5109, 2012.

Rixen, T., Baum, A., Gaye, B., and Nagel, B.: Seasonal and interannual variations in the nitrogen cycle in the Arabian Sea, Biogeosciences, 11, 5733-5747, 2014.

Rixen, T., Guptha, M. V. S., and Ittekkot, V.: Deep ocean fluxes and their link to surface ocean processes and the biological pump, Progress in Oceanography, 65, 240-259, 2005.

Rixen, T. and Ittekkot, V.: Nitrogen deficits in the Arabian Sea, implications from a three component mixing analysis, Deep-Sea Research Part II-Topical Studies in Oceanography, 52, 1879-1891, 2005.

Rohling, E. J. and Zachariasse, W. J.: Red Sea outflow during the last glacial maximum, Quaternary International, 31, 77-83, 1996.

Biogeosciences Discuss., https://doi.org/10.5194/bg-2017-256
Manuscript under review for journal Biogeosciences
Discussion started: 27 June 2017

Rostek, F., Bard, E., Beaufort, L., Sonzogni, C., and Ganssen, G.: Sea surface temperature and productivity records for the past 240 kyr in the Arabian Sea, Deep-Sea Research, 44, 1461-1480, 1997.

Saraswat, R., Lea, D. W., Nigam, R., Mackensen, A., and Naik, D. K.: Deglaciation in the tropical Indian Ocean driven by interplay between the regional monsoon and global teleconnections, Earth and Planetary Science Letters, 375, 166-175, 2013.

Saraswat, R., Nigam, R., Weldeab, S., Mackensen, A., and Naidu, P. D.: A first look at past sea surface temperatures in the equatorial Indian Ocean from Mg/Ca in foraminifera, Geophysical Research Letters, 32, 4, 2005.

Sarma, V.: An evaluation of physical and biogeochemical processes regulating perennial suboxic conditions in the water column of the Arabian Sea, Global Biogeochemical Cycles, 16, 11, 2002.

Schlitzer, R.: Ocean Data View, http://odv.awi.de, 2016.

Schmittner, A., Galbraith, E. D., Hostetler, S. W., Pedersen, T. F., and Zhang, R.: Large fluctuations of dissolved oxygen in the Indian and Pacific oceans during Dansgaard-Oeschger oscillations caused by variations of North Atlantic Deep Water subduction, Paleoceanography, 22, 17, 2007.

Schmittner, A. and Somes, C. J.: Complementary constraints from carbon (C-13) and nitrogen (N-15) isotopes on the glacial ocean's soft-tissue biological pump, Paleoceanography, 31, 669-693, 2016.

Schulte, S. and Muller, P. J.: Variations of sea surface temperature and primary productivity during Heinrich and Dansgaard-Oeschger events in the northeastern Arabian Sea, Geo-Marine Letters, 21, 168-175, 2001.

Siddall, M., Rohling, E. J., Almogi-Labin, A., Hemleben, C., Meischner, D., Schmelzer, I., and Smeed, D. A.: Sea-level fluctuations during the last glacial cycle, Nature, 423, 853-858, 2003.

Sigman, D., Karsh, K. L., and Casciotti, K. L.: Ocean process tracers: Nitrogen isotopes in the ocean. In: Encyclopedia of Ocean Sciences (update from 2001), Steele, J. H., Turekian, K. K., and Thorpe, S. A. (Eds.), Academic Press, London, 2009.

Sirocko, F., Garbe-Schönberg, D., and Devey, C.: Processes controlling trace element geochemistry of Arabian Sea sediments during the last 25,000 years, Global and Planetary Change, 26, 217-303, 2000.

Sonzogni, C., Bard, E., Rostek, F., Dollfus, D., Rosell-Melé, A., and Eglinton, G.: Temperature and Salinity Effects on Alkenone Ratios Measured in Surface Sediments from the Indian Ocean, Quaternary. Research, 47, 344-355, 1997a.

Sonzogni, C., Bard, E., Rostek, F., Lafont, R., Rosell-Mele, A., and Eglinton, G.: Core-top calibration of the alkenone index vs sea surface temperature in the Indian Ocean, Deep Sea Research Part II: Topical Studies in Oceanography, 44, 1445-1460, 1997b.

Stern, J. V. and Lisiecki, L. E.: Termination 1 timing in radiocarbon-dated regional benthic $\delta^{18}O$ stacks, Paleoceanography, 29, 1127-1142, 2014.

Suresh, I., Vialard, J., Izumo, T., Lengaigne, M., Han, W., McCreary, J., and Muraleedharan, P. M.: Dominant role of winds near Sri Lanka in driving seasonal sea level variations along the west coast of India, Geophysical Research Letters, 43, 7028-7035, 2016.

Suthhof, A., Ittekkot, V., and Gaye-Haake, B.: Millennial-scale oscillation of denitrification intensity in the Arabian Sea during the late Quaternary and its potential influence on atmospheric N_2O and global climate, Global Biogeochemical Cycles, 15, 637-650, 2001.

Tierney, J. E., Pausata, F. S. R., and deMenocal, P.: Deglacial Indian monsoon failure and North Atlantic stadials linked by Indian Ocean surface cooling, Nature. Geoscience, 9, 46-50, 2016.

Tiwari, M., Ramesh, R., Bhushan, R., Sheshshayee, M. S., Somayajulu, B. L. K., Jull, A. J. T., and Burr, G. S.: Did the Indo-Asian summer monsoon decrease during the Holocene following insolation?, Journal of Quaternary Science, 25, 1179-1188, 2010.

Tiwari, M., Nagoji, S. S., and Ganeshram, R. S.: Multi-centennial scale SST and Indian summer monsoon precipitation variability since the mid-Holocene and its nonlinear response to solar activity, Holocene, 25, 1415-1424, 2015.

Vijith, V., Vinayachandran, P. N., Thushara, V., Amol, P., Shankar, D., and Anil, A. C.: Consequences of inhibition of mixed-layer deepening by the West India Coastal Current for winter phytoplankton bloom in the northeastern Arabian Sea, Journal of Geophysical Research-Oceans, 121, 6583-6603, 2016.

Wiggert, J. D., Jones, B. H., Dickey, T. D., Brink, K. H., Weller, R. A., Marra, J., and Codispoti, L. A.: The northeast monsoon´s impact on mixing, phytoplankton biomass and nutrient cycling in the Arabian Sea, Deep-Sea Research II, 47, 1353-1385, 2000.

Yoshinari, T., Altabet, M. A., Naqvi, S. W. A., Codispoti, L., Jayakumar, A., Kuhland, M., and Devol, A.: Nitrogen and oxygen isotopic composition of N_2O from suboxic waters of the eastern tropical North Pacific and the Arabian Sea - measurement by continuous-flow isotope-ratio monitoring, Marine Chemistry, 56, 253-264, 1997.

Biogeosciences Discuss., https://doi.org/10.5194/bg-2017-256
Manuscript under review for journal Biogeosciences
Discussion started: 27 June 2017

Biogeosciences Discussions Open Access EGU

Table 1:

Table 1: Core names, locations, depths, references, and variables used; SST A indicate alkenone temperatures and SST Mg/Ca indicate temperatures based on Mg/Ca ratios

Core	Latitude	Longitude	Depth [m]	Reference	Variables
SO90-39KG	24.8335N	65.9168E	695	Böll et al. 2014	SST A, $\delta^{15}N$
SO130-275KL	24.8218N	65.9100E	782	Böll et al. 2014	SST A, $\delta^{15}N$
SO90-93KL	23.5833N	64.2167E	1802	Böll et al. 2015	SST A
SO90-136KL	23.1223N	66.4972E	568	Schulte and Müller 2001	SST A
M74-SL163	21.9328N	59.8025E	650	this study	SST A, $\delta^{15}N$
MD 00-2354	21.0425N	61.475166E	2740	Böll et al. 2015	SST A
RC27-42	16.5N	59.8E	2040	Pourmand et al. 2007	SST A
SO42-74KL	14.3210N	57.3470E	3212	Huguet et al. 2006; Suthhof et al. 2002	SST A, $\delta^{15}N$
TY93-929	13.1223N	53.25E	2490	Rostek et al. 1997	SST A
MC2/GOA4	12.8215N	46.921666N	1474	Isaji et al., 2015	SST A, $\delta^{15}N$
MD90963	5.066666N	73.8833E	2450	Rostek et al. 1997	SST A
MD85674	3.18333N	50.43333E	4875	Bard et al. 1997	SST A
SK117/GC-08	15.4833N	71.0E	2500	Banakar et al. 2010	SST Mg/Ca, $\delta^{15}N$
AAS9/21	14.6666N	72.4833E	1807	Govil and Naidu 2010	SST Mg/Ca
SN-06	12.4854N	74.1265E	589	Tiwari et al. 2015	SST Mg/ca
P178-15P	11.955N	44.3E	869	Tierney et al. 2016	SST A
SK237-CG04	10.9775N	74.999333E	1245	Saraswat et al. 2013	SST Mg/Ca
SK129/CR04	6.4833N	75.96667E	2000	Mahesh and Banakar 2014	SST Mg/Ca
NIOP-905P	10.76666N	51.9500E	1586	Huguet et al. 2006	SST A
SK157-4	02.66667N	78.0E	3500	Saraswat et al. 2005	SST Mg/Ca
MD85668	-0.01667S	46.0833E	4020	Rostek et al. 1997	SST A
MD 04-2876	24.842833N	64.008167E	828	Pichevin et al. 2007	$\delta^{15}N$
NIOP455	23.5506N	65.95E	1002	Reichart et al. 1998	d15N
SO90-111KL	23.0766N	66.4836E	775	Suthhof et al. 2002	$\delta^{15}N$
MD04-2879	22.5483N	64.0467E	920	Jaeschke et al. 2009	$\delta^{15}N$
M74-MC680	22.6193N	59.6916E	789	this study	$\delta^{15}N$
NIOP 464	22.2506N	63.5836E	1470	Reichart et al. 1998	$\delta^{15}N$
NAST	19.999N	65.6843E	3170	Möbius et al. 2011	$\delta^{15}N$
ODP724C	18.2833N	57.4667E	600	Möbius et al. 2011	$\delta^{15}N$
RC27-14	18.25333N	57.6550E	596	Altabet et al. 2002	$\delta^{15}N$
RC27-23	17.993333N	57.5900E	820	Altabet et al. 2002	$\delta^{15}N$
ODP 722B	16.6167N	59.8E	2028	Möbius et al. 2011	$\delta^{15}N$
EAST	15.5917N	68.5817E	3820	Möbius et al. 2011	$\delta^{15}N$
MD76-131	15.53N	72.5683E	1230	Ganeshram et al. 2000	$\delta^{15}N$
CR-2	14.9N	74E	45	Agniihotri et al., 2008	$\delta^{15}N$
MC2-GOA6	14.9800N	53.767333E	2416	Isaji et al., 2015	$\delta^{15}N$
SS4018G	13.2133N	53.2567E	2830	Tiwari et al. 2010	$\delta^{15}N$
SK126-39	12.63N	73.33E	1940	Kessarkar et al. 2010	$\delta^{15}N$
SS3268G5	12.5N	74.2E	600	Agnihotri et al., 2003	$\delta^{15}N$
NIOP-905P	10.76666N	51.9500E	1586	Ivanchko et al. 2005	$\delta^{15}N$

Figure Caption:

Figure 1: Stations of sediment cores for SST (a) and $\delta^{15}N$ reconstructions (b) with colors indicating: surface sediment samples (purple); cores from the Oman Upwelling (dark blue); Somali Upwelling (light blue); the western (green); northern (yellow), eastern (red), and southeastern (orange) Arabian Sea.

Figure 2: SST in °C from Jan-Mar (NE-monsoon) (a), and Jul-Sep (SW-monsoon) (b) from the World Ocean Atlas (1955-2012). Solid arrows indicate major wind directions and broken arrows indicate surface general currents; WICC = West Indian Coastal Current.

Fig. 3: Millennial regional averages of SST [°C] and ±1 δ standard deviation in the northern, eastern, and western Arabian Sea, in the Oman and Somali upwelling areas and the southeastern Arabian Sea of the last 25 ka. Regions are indicated in Figure 1.

Fig: 4: Annual SST distribution in °C (1955-2012) from the World Ocean Atlas (a), alkenone and Mg/Ca derived SST reconstruction for the time slice from 17-18 ka BP (b) from cores shown in Figure 1.

Fig: 5: $\delta^{15}N$ in ‰ in recent surface sediments (a); $\delta^{15}N$ in sediments at 17-18 ka BP (b) from surface and core locations shown in Figure 1.

Fig. 6: $\delta^{18}O$ record from the GISP2 ice core (Grootes and Stuiver, 1997) and sea level reconstruction from the Red Sea (Siddall et al., 2003) (a), compared with millennial regional averages of normalized and averaged $\delta^{15}N$ values from the northern (b), eastern (c), and western (d) Arabian Sea, the Oman (e), and Somali (f) upwelling and area, and total organic carbon mass accumulation in the Arabian Sea (TOC MAR; data from Cartapanis et al., 2016, and T. Rixen, unpublished) and insolation at 30°N in W m^{-2} (Berger and Loutre, 1991) (g) during the last 25 ka,. Error bars denote ±1 δ.

Fig. 7: Millennial regional average SST from the northern Arabian Sea minus Oman Upwelling average SST (black line) and northern Arabian Sea minus Somali Upwelling average SST (red line; regions are indicated in Figure 1.), compared with reconstructions of the mean effective moisture in southern and central Asia (blue line) and the Indian monsoon region (green line) from continental archives (Herzschuh, 2006).

Figure 8: Simulated volume of the Arabian Sea OMZ (70 µmol l^{-1} threshold, black) and export production in the entire Arabian Sea (red), western Arabian Sea (green) and eastern Arabian Sea (blue) over the Holocene (upper panel) and OMZ volume and age of water masses (time since contact with the surface) averaged over the OMZ (lower panel). Arabian Sea defined as 55°E-75° E, 8.5°N-22.5° N, border between west and east defined at 68.5° E.

Biogeosciences Discuss., https://doi.org/10.5194/bg-2017-256
Manuscript under review for journal Biogeosciences
Discussion started: 27 June 2017

Figure 1:

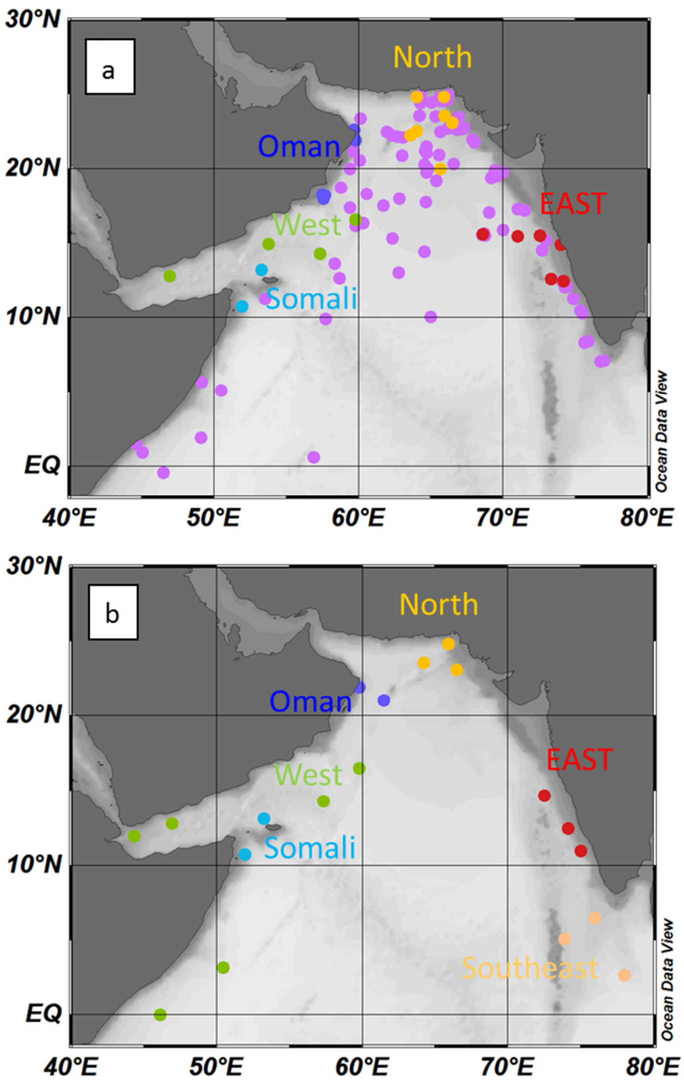

Biogeosciences Discuss., https://doi.org/10.5194/bg-2017-256
Manuscript under review for journal Biogeosciences
Discussion started: 27 June 2017

Figure 2:

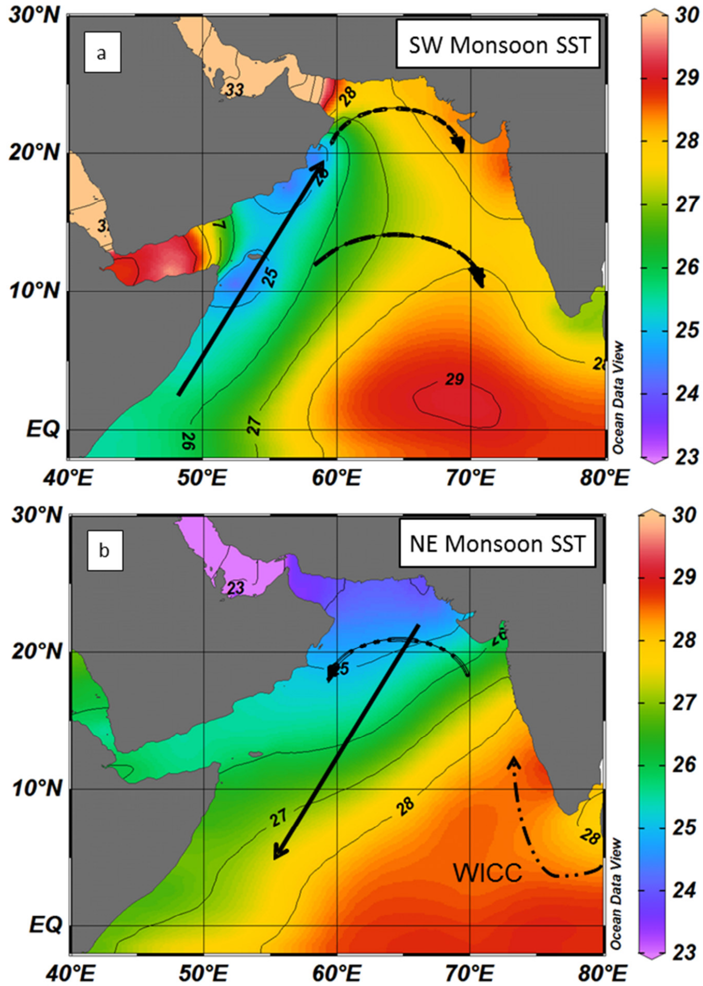

Fig. 3:

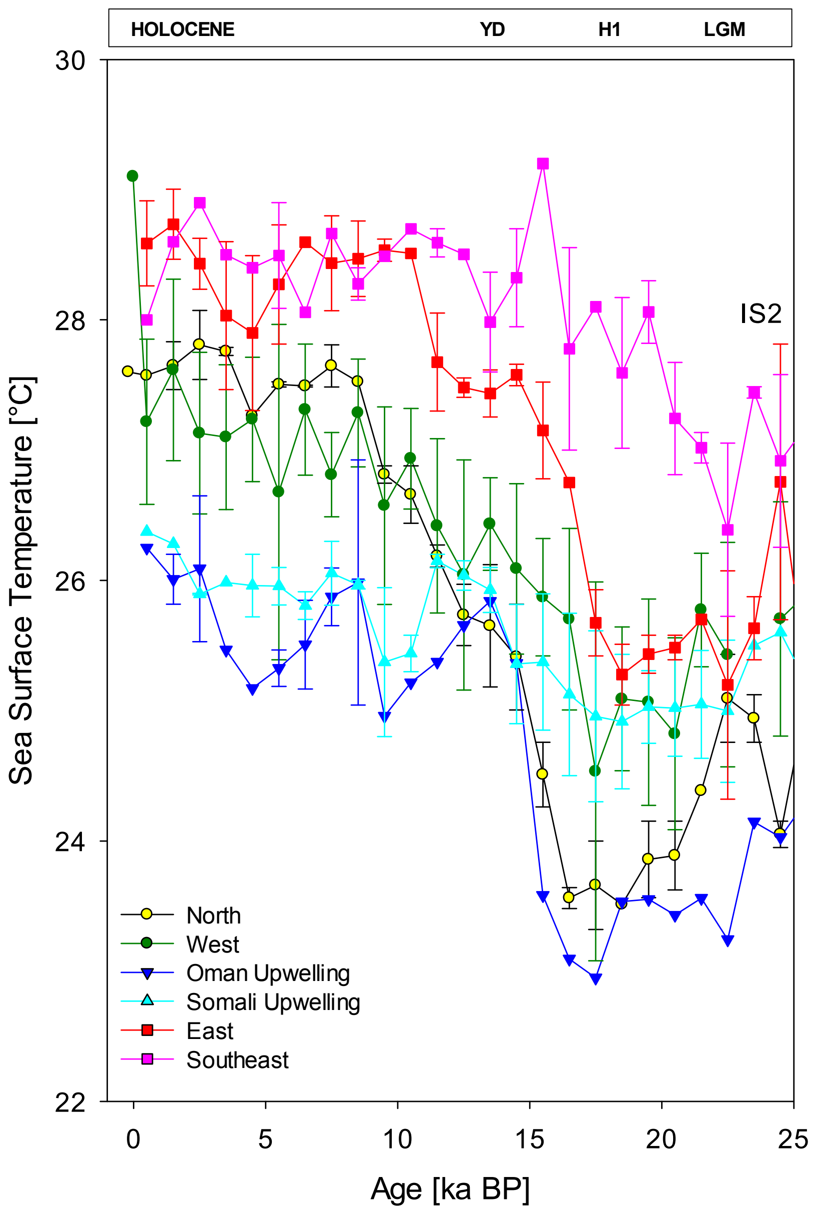
HOLOCENE
YD
H1
LGM
IS2
Sea Surface Temperature [°C]
30
28
26
24
22
0
5
10
15
20
25
Age [ka BP]
North
West
Oman Upwelling
Somali Upwelling
East
Southeast

Biogeosciences Discuss., https://doi.org/10.5194/bg-2017-256
Manuscript under review for journal Biogeosciences
Discussion started: 27 June 2017

Fig: 4:

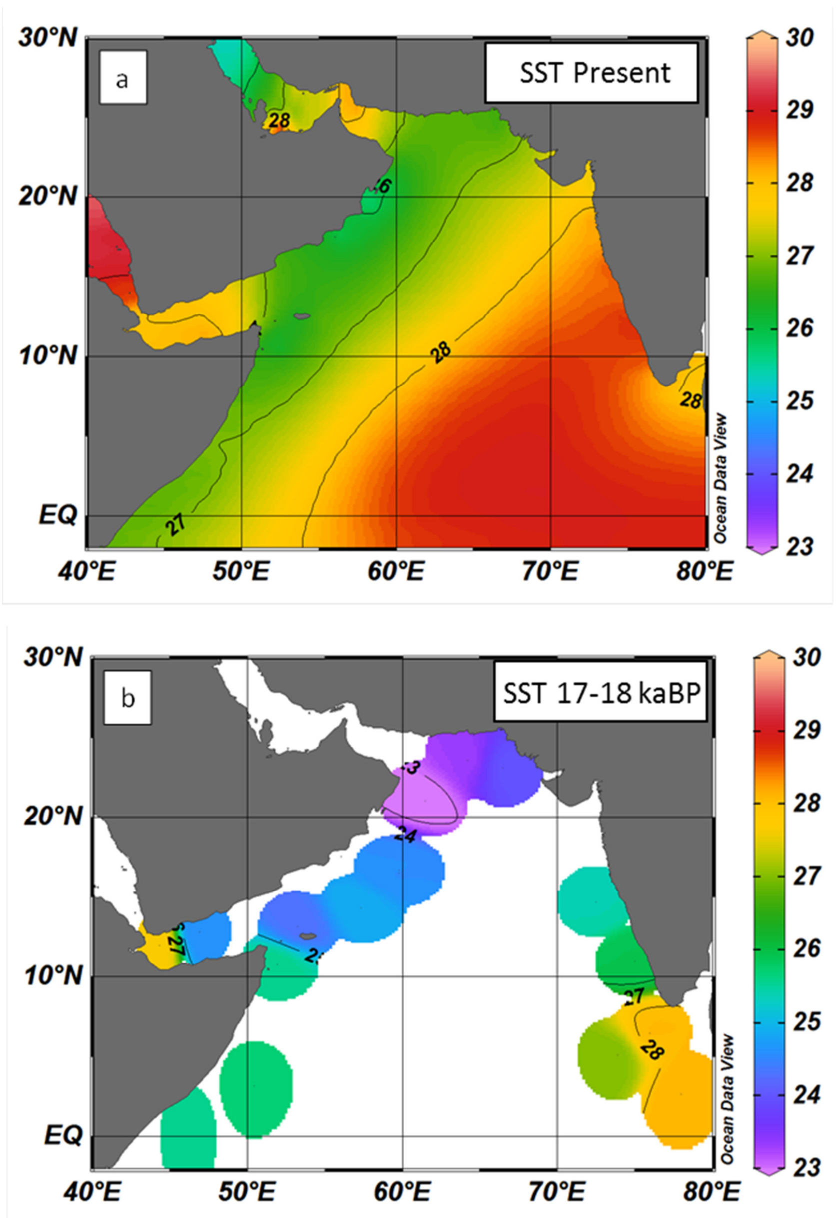

Biogeosciences Discuss., https://doi.org/10.5194/bg-2017-256
Manuscript under review for journal Biogeosciences
Discussion started: 27 June 2017

929 Fig. 5:

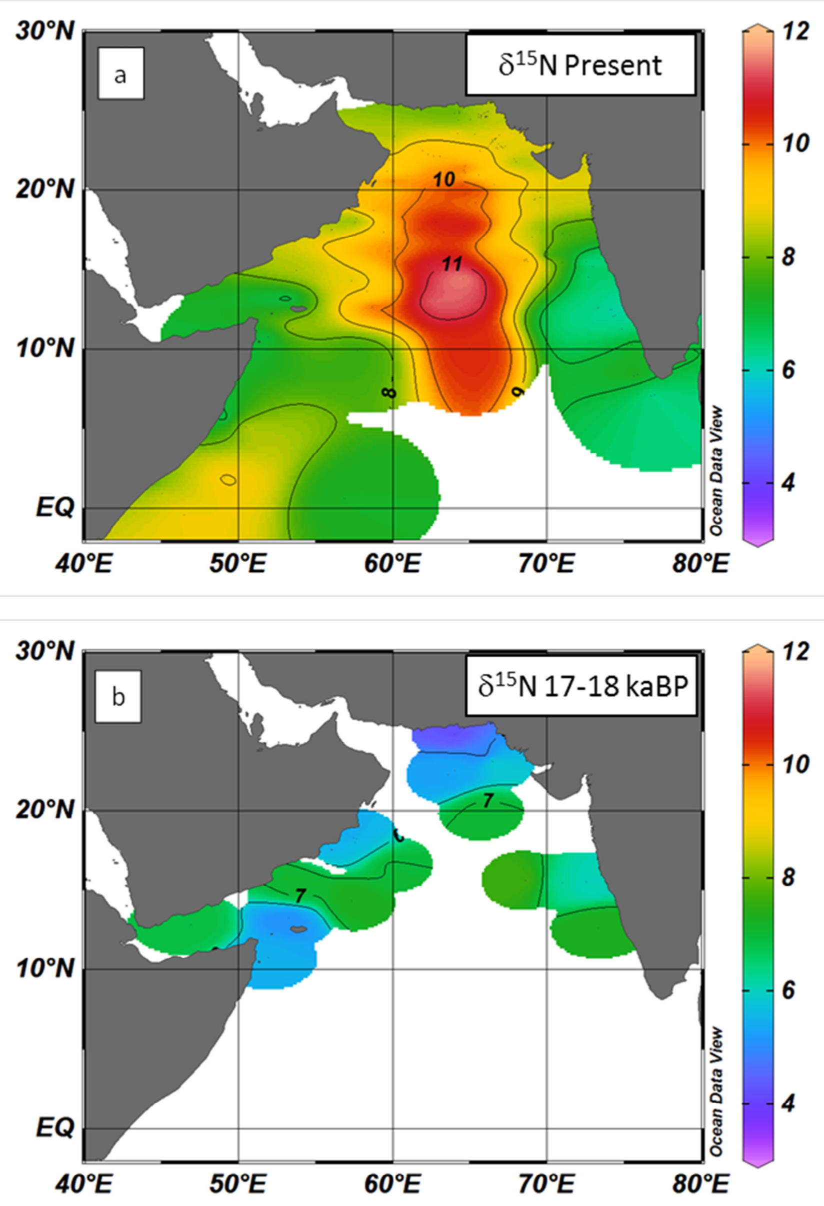

930

931

Fig. 6:

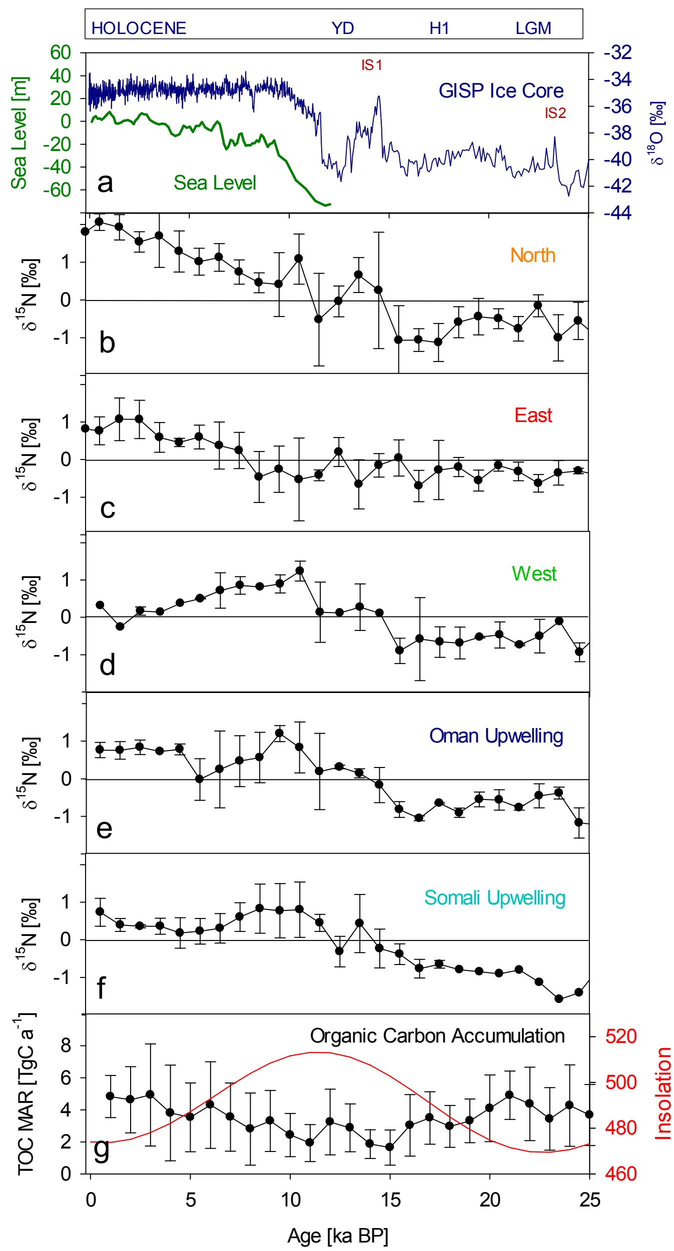
HOLOCENE
YD
H1
LGM
IS1
IS2
GISP Ice Core
Sea Level
Sea Level [m]
δ18O [‰]
a
North
b
East
c
West
d
Oman Upwelling
e
Somali Upwelling
f
δ15N [‰]
Organic Carbon Accumulation
g
TOC MAR [TgC a-1]
Insolation
Age [ka BP]

936 Fig. 7:

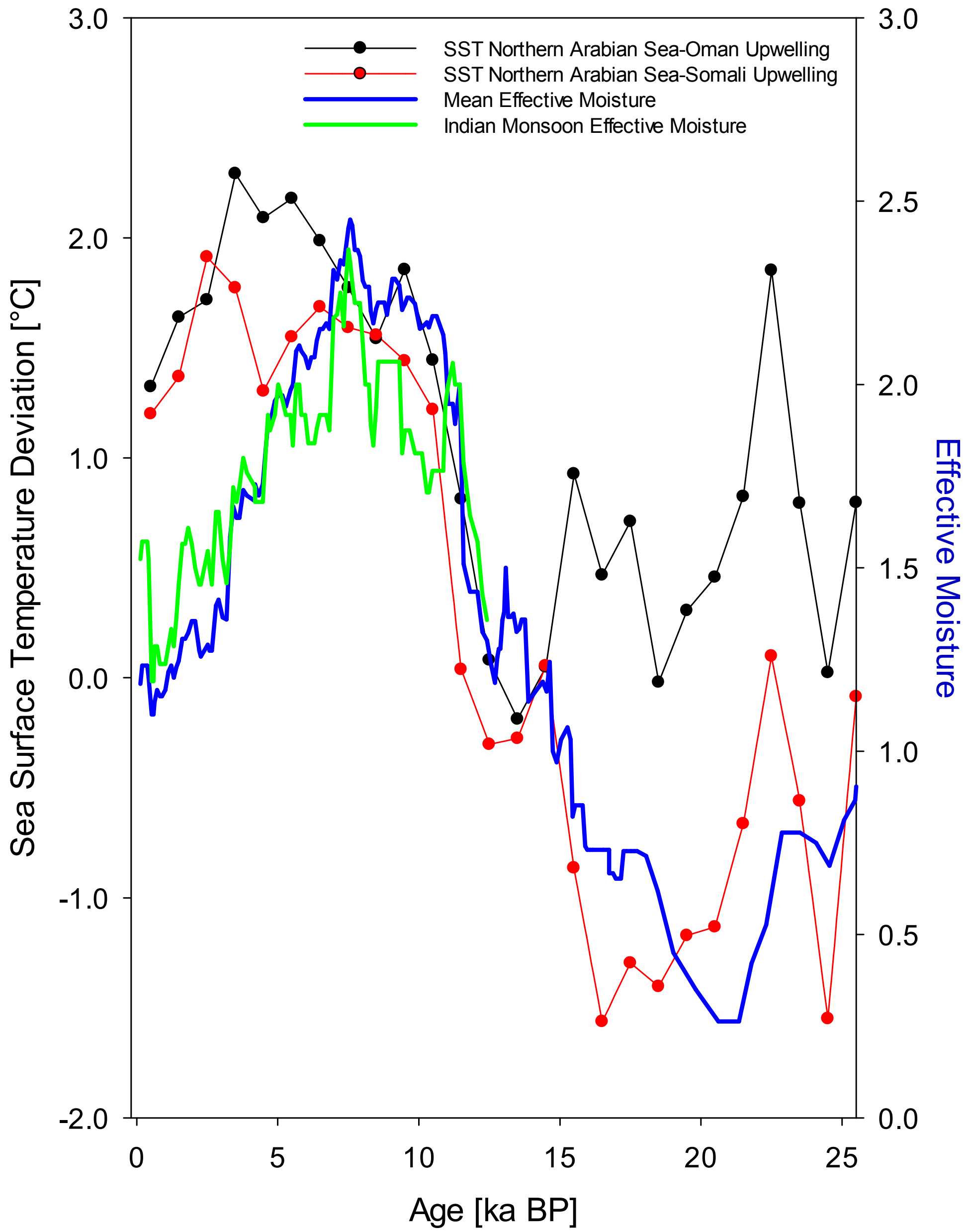

937

938

Biogeosciences Discuss., https://doi.org/10.5194/bg-2017-256
Manuscript under review for journal Biogeosciences
Discussion started: 27 June 2017

Figure 8: